A R C H I V E O F M E C H A N I C A L E N G I N E E R I N G

Volume 66 2019 Number 1

DOI: 10.24425/ame.2019.126375

Key words: SHM, fiber optic, genetic optimization, strain energy

Salvatore Ameduri[1], Monica Ciminello[1], Ignazio Dimino[1], Antonio Concilio[1], Alfonso Catignani[2], Raimondo Mancinelli[2]

Distributed sensor placement optimization for computer aided structural health monitoring

An optimal sensor placement methodology is implemented and herein proposed for SHM model-assisted design and analysis purposes. The kernel of this approach analysis is a genetic-based algorithm providing the sensor network layout by optimizing the probability of detection (PoD) function while, in this preliminary phase, a classic strain energy approach is adopted as well established damage detection criteria. The layout of the sensor network is assessed with respect to its own capability of detection, parameterized through the PoD. A distributed fiber optic strain sensor is adopted in order to get dense information of the structural strain field. The overall methodology includes an original user-friendly graphical interface (GUI) that reduces the time-to-design costs needs. The proposed methodology is preliminarily validated for isotropic and anisotropic elements.

1. Introduction

Different challenges shall be faced for implementing Structural Health Monitoring (SHM) systems on real structures, because of their typical large size and complexity and the possibility of working during operations (real-time systems). Such constraints drive the selection of the monitoring hardware and software, and often result in the need of a dense array of high-fidelity sensors. For all those reasons, cost and cabling is certainly an issue. The high interest and potential for the practical application of SHM is stimulating research for identifying more compact and economic solutions, while maintaining or even increasing the overall system performance. In this case, massive data stream is a concern: extensive information

✉ Salvatore Ameduri, email: s.ameduri@cira.it

[1]Centro Italiano Ricerche Aerospaziali, CIRA, Capua, Italy.

[2]Universitá degli Studi di Napoli 'Federico II', Napoli, Italy.

can inundate the end-user without providing any real advantage. In addition, SHM systems are preferred to be conservative [1, 2]: it is accepted they reveal a false damage instead than neglecting an actual one. In this sense, such systems may be characterized by their intrinsic Probability of Detection (PoD) capability, expressing the chance to detect a damage of a certain size within the target structure. An experimental assessment of such a capability is very expensive, because of the large number of trials to be performed in order to have a statistically valid dataset; the numerical way is therefore preferred. Within this frame, a computer-assisted methodology is herein implemented and proposed for SHM system cost effective design and analysis purposes; optimal sensor placement is a key issue for this aim.

Optimal sensor placement can be based on modal tests. The basic idea of this methodological approach is that damage sensitivities in the established domains are calculated, based on modal parameters [3–5]. Then, the most responsive elements are selected, according to a certain criterion. Their minimal number can be established through a dedicated analysis. Optimal sensor placement technique plays a key role also in [6] where the sensor layout aims at maximizing the potentiality of characterizing the structural dynamic behavior. An improved genetic algorithm is therein introduced to point out the best sensors distribution, based, again, on modal test criteria. Modal strain energy (MSE) and modal assurance criterion (MAC) are taken as fitness functions, alternatively. A comparison criterion based on the mean square error between the finite element method (FEM) and the Guyan expansion mode shapes, identified by data-driven stochastic subspace identification method, are employed to demonstrate the advantages of the different fitness functions [7].

In the last two decades, the use of optical fibers and related optical components is dramatically increased, accompanied by the development of a large variety of related sensors with the perspective of realizing cheaper and lighter networks with a reduced impact in terms of cabling. For instance, distributed sensing systems [8] allow using standard, inexpensive telecom fibers. In that case, the fiber itself becomes the sensor, the associated interrogator system being able to detect changes in their physical characteristics for tens of meters with a very high resolution [9, 10].

In [11] a unified sensor performance metric is defined for vibrations monitoring and fault detection as the integration of a weighted functional of some strain measures over the optical fiber length for both discrete and distributed sensors. The optical fiber is represented by a non-uniform rational B-spline curve. The design variables include specific control points and arc length coordinates of the sensing elements along the fiber. Constraints include the max fiber length and the max allowed curvature, parameters that are commonly associated to optical sensors. For distributed fiber-optic sensors, a genetic algorithm-based solver to optimally connect sensors using one single optical fiber by minimizing the total fiber length.

In this study, a novel optimal sensor placement strategy based on strain energy sensitivity is proposed, for distributed, high-density fiber-optic sensors. The kernel of this analysis is a genetic-based algorithm that provides the optimal layout by maximizing the PoD function, while a classic approach [12–14] is adopted

as the established reference damage detection criterion. Other approaches could, however, be selected [15]. The methodology includes a user-friendly graphical interface (GUI) that reduces the time-to-design needs [16–18]. The proposed tool is experimentally validated through two different applications, metallic and stiffened laminate plates of aeronautical interest.

2. Methodology outline

The target of the genetic optimization was to find out a spatial distribution of strain sensors, that could maximize the PoD of a spot damage, potentially occurring on the entire plate. To this scope a database was built, correlating the generic positions of the damages to the strain energy onto the entire plate. In practice, a statistically significant number (500) of potential locations of the damages was generated. Per each damage, a dedicated procedure was implemented to modify the plate model and to run a modal analysis for reconstructing the strain distribution onto the plate. The assessed database was used as input for the genetic algorithm. The approach, adopted for the optimization and illustrated in Fig. 1, includes the steps below:

1. *Generation of the locations (abscissas and ordinates) of the sensors onto the plate*. Each x and y coordinate represents a chromosome of the algorithm, ranging along the entire in-plane dimensions of the plate. It is worth to note that in the specific case of fiber optic sensors, another important aspect is the slope at which the fiber crosses the points, since the strain is measured only in that direction. This component, part of the local strain tensor $\boldsymbol{\varepsilon}'$, can be extracted by the global strain tensor $\boldsymbol{\varepsilon}$, using the following equation

$$\boldsymbol{\varepsilon}' = Q\boldsymbol{\varepsilon}Q^T \tag{1}$$

being Q the rotation matrix, in turn function of the local slope ϑ

$$Q = \begin{bmatrix} \cos\vartheta & -\sin\vartheta \\ \sin\vartheta & \cos\vartheta \end{bmatrix}. \tag{2}$$

If the minimum curvature radius of the spline is higher than the threshold structural limit of the fiber (15 mm) and, in the case of a composite stiffened panel, no intersections with the bonding line are found, the next step is faced; in case this constraints are not met, the PoD is set to 0, skipping the steps 2 and 3. The check on the curvature, however, is not performed in case of a pre-programmed path for the fiber, as for the second test case considered in this work (anisotropic plate integrated with stringers), in which linear paths were assumed. The interference check prevents from sudden curvature variations of the fiber, due to the necessity of a sharpen override in out-of plane direction, to avoid the stringer step.

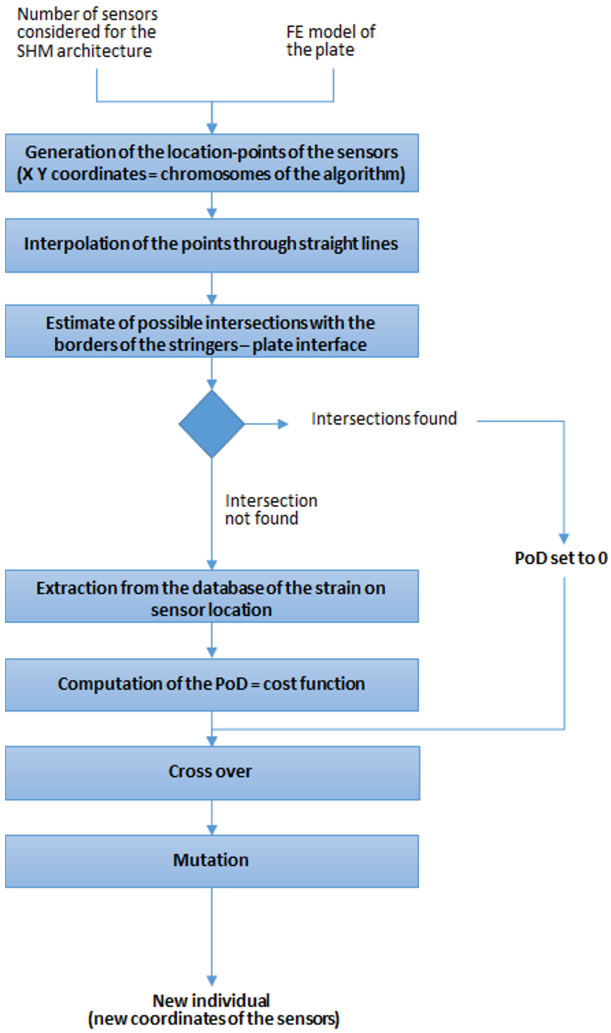

Fig. 1. Flow chart of the optimization process for the metallic (isotropic) and the composite (anisotropic) plate

Finally, in principle, the intersection of the fiber optic path representative spline with itself could have been also checked, but from a practical point of view, this condition may be faced just overlapping the fiber.
It is worth to note that the sequence of the sensors is defined by the point generation order.

2. *Estimate of the strain at the locations of the sensors*. This task is performed by interpolating the strain distribution stored in the database for each of the damages considered. The strain components along the abscissa and the ordinate axes is projected along the local direction of the fibre.

3. *PoD estimate*. The PoD is then computed implementing the process described in the next section. This value is assumed as cost function.
4. *Crossover*. The population, constituted by the different sets of sensors then undergoes the cross-over process: some chromosomes (sensor locations) of single individuals are exchanged with the corresponding ones of other individuals, thus generating a different population. The individuals and the chromosomes subject to this process are chosen on the basis of a probabilistic law that privileges the exchange between individuals characterized by higher PoD values. In any case, the genetic heritage of the best individual is preserved.
5. *Mutation*. Some individuals of the new population undergo a spontaneous (random) mutation of part of their heritage, to enrich the genetic content of the population and to avoid premature convergences

Due to the heuristic nature of the optimization strategy and with the specific aim of preventing immature convergences, several runs were carried out, starting from different initial populations (that is to say, set of sensor coordinates) also characterized by different number of sensors. With this approach and in the limit of the heuristic nature of the process, a correlation has been assessed between the number of sensors and achieved PoD.

The two processes, the one for the metal plate without additional structural elements and the other one for the anisotropic plate with the two stringers are illustrated in the following figure.

2.1. PoD estimation

The modal strain energy U_i, linked to the i-th mode, in the case of an isotropic plate, can be expressed as function of the normal displacement w_i of the same mode:

$$U_i = \frac{D}{2} \int_0^{L_y} \int_0^{L_x} \left(\frac{\partial^2 w_i}{\partial x^2} + \frac{\partial^2 w_i}{\partial y^2} \right)^2 - 2(1-\nu) \left(\frac{\partial^2 w_i}{\partial x^2} \frac{\partial^2 w_i}{\partial y^2} - \left(\frac{\partial^2 w_i}{\partial x \partial y} \right)^2 \right) \mathrm{d}x \, \mathrm{d}y \tag{3}$$

being D the bending stiffness, ν the Poisson modulus and L_x and L_y the in plane dimensions of the plate. This strain modal energy can be expressed as summation of the energies associated to n single sub-regions, the domain is split into:

$$U_i = \sum_j^n U_{ij} \, . \tag{4}$$

In this work, each finite element represents a sub region and the corresponding strain energy is computed from the local strain field. The size of the element was

chosen to assure an adequate representation of the sensor gauge length. In the case of a fiber Bragg grating, the in plane dimensions of the plate element (square) is equal to the grating extension, while, for the case of a distributed fiber sensor, the size of the element amounts to the discrete representation of the strain acquired.

For the case of a partial acquisition of strain (in case of the fiber sensor, the component along the tangent direction), the U_{ij} terms represent only a portion of energy, computed through the available measured strain component.

According to [10], defining the sub-region indexes, β_j as ratio of the sum of the fractional energy for the m lowest observed modes in a sub-region j of the damaged (d) and undamaged (u) structure

$$\beta_j = \frac{\sum_{i=1}^{m} \frac{U_{ij}^d}{U_i^d}}{\sum_{i=1}^{m} \frac{U_{ij}^u}{U_i^u}} \tag{5}$$

the associated damage index DI_j can be expressed as it follows:

$$\mathrm{DI}_j = z_j = \frac{\beta_j - \mu_\beta}{\sigma_\beta} \tag{6}$$

being z_j the standard score and representing the number of standard deviations σ_β away from the mean μ_β. It is worth to note that this method better addresses low frequency ranges and structures that exhibit a low modal density.

An arbitrary confidence interval may be defined ($z > 2$) which provides an indication of the damage presence. Based on a population of found and missed damage, via DI alert, a PoD function can be hence estimated.

$$\mathrm{PoD} = \frac{\text{Number of damage detected}}{\text{Total number of damage}}\,. \tag{7}$$

3. Graphical User Interface

From the finite element model of the target structure, a set of modal parameters is extracted. Then, random damage set can be defined in terms of shape, size and number, through a user-friendly GUI. Once this numerical operation is completed and the reference dataset has been built, the GUI is again used for the sensors network distribution. Such a software is developed in Python, programming language widely used for this kind of applications, thanks to its object-oriented architecture, providing high stability and velocity in writing and reading files. The GUI allows the kernel to interface with MSC/Nastran models. After the reference structure is imported as a bulk data file, it is possible to implement certain types of damage, like local delamination and de-bonding. The damage dimensions are set by modifying

the model property cards. Delamination is simulated trough a stiffness reduction of material (MAT cards) or redefining the stacking sequence of the damaged zone (plies number, thickness, stiffness, etc.; PCOMP card). De-bonding is instead simulated by removing CBUSH or RBE elements within the area of interest, simulating the adhesive or connection failure. Random multiple damage spot can be generated (Fig. 2) for the optimization process.

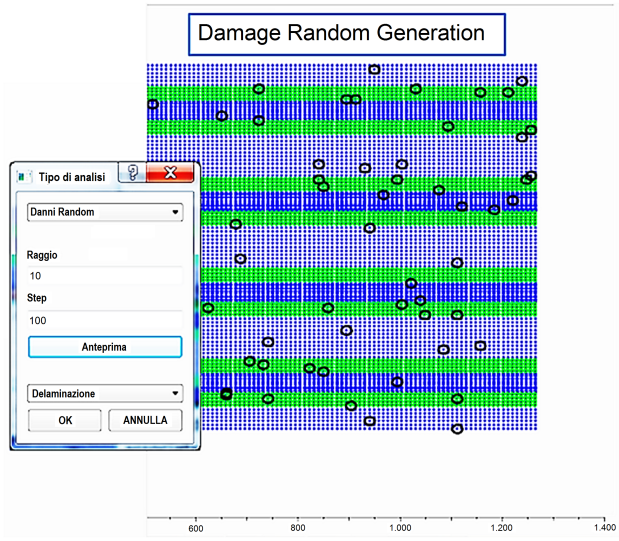

Fig. 2. Generation of a random layout of circular damage on a stiffened composite plate

In-plane strains and curvatures are selected (Fig. 3) to compute a damage index (DI), based on the strain energy evaluation (see Eq. (2)). The data reported in the Nastran output file are used to generate the component of the strain along the local

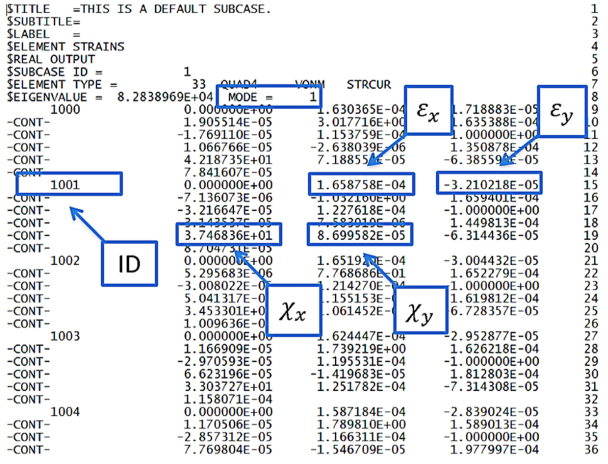

Fig. 3. Output file providing post processed strain and curvature

fiber direction. More in detail, the tensile strain components on the mid plane, ε_x and ε_y and the corresponding curvatures χ_x and χ_y are elaborated, through a dedicated procedure, to produce the surface global strain that is in turn elaborated using (1) and (2) to produce the strain along the fiber direction.

4. Isotropic test case: aluminum plate

A simple aeronautical aluminum (72 GPa) plate is considered. The plate dimensions are 600×200 mm and its thickness is 0.5 mm. The damage condition is produced by an impact at a low-energy level (> 50 J).

The structural element has been meshed with an adequate resolution (squares of 10×10 mm comparable to a Barely Visible Damage dimension, BVID). Each of them represents a possible location of a single strain sensor.

Eight different random sensor networks have been considered, different for the total number of sensors, ranging from 6 to 13. The first 4 normal modes have been considered. For each configuration, the PoD has been maximized by means of the genetic algorithm.

Ten initial populations (corresponding to the times the optimization process was run) were random generated per each of the considered sensor networks. Each run has foreseen 100 iterations leading to the generation of new populations, through cross-over and mutation processes. Each population is constituted by 100 individuals, whose heritage is represented by the (xy) coordinates (namely chromosomes) of the sensors. The cross-over process implies the exchange of half the coordinates between two individuals. The mutation produces small alterations (up to 5%) of no more than 1 chromosome of the 10% of the individuals.

The database cited in section 2 has been built considering random distributions of damage. More in details, 1 damaged finite element every 100 elements has been assumed and randomly generated. To make an example, for a total of 1000 elements (potential locations of the damage) only 10 have been random assumed damaged. In this case, local mass or stiffness variations due to impact are simulated. The optimal configurations for 6 and 13 sensors are reported in Fig. 4 and Fig. 5, together with the max value of PoD during iterations (convergence feature).

With reference to the configuration with 6 sensors, the different optimizations proved the impossibility of achieving a PoD of 100%; to support this result, the fitness for different runs have been illustrated in the same figure. The final distribution of the sensors does not reflect a modal shape oriented configuration, since their number is not enough to guarantee an adequate covering of the domain. PoD greater than 99% have been obtained only for configurations with a sensors number exceeding 9. Furthermore, the convergence velocity increased as the sensors number grew. The 13-sensor configuration has been selected as the optimal amongst the investigated ones. An idea of the robustness of this solution (13 sensors) is given by the plot of Fig. 6, reporting the max PoD for a number of sensors ranging from 6 to 13. According to the sensor network provided by the genetic algorithm (Fig. 5),

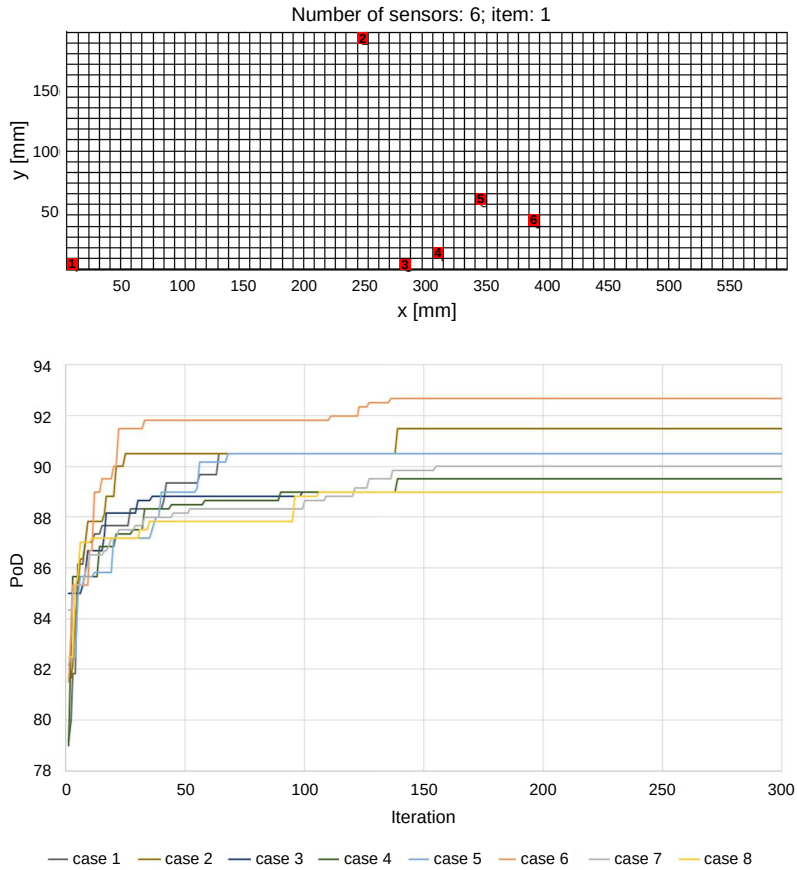

Fig. 4. Optimized configurations and PoD evolutions for 6 sensors

a distributed fiber optic is used to instrument the plate. The 2 m long fiber optic (dotted line in Fig. 7), allows for a full covering of the optimal sensing locations (star dots in Fig. 7). It is clear that the fiber optic layout is compliant with the 13 optimized sensing points.

In order to provide an experimental validation of the introduced methodology, the plate has been random impacted 6 times and then excited by a PZT externally bonded on the opposite surface of the plate; free-free constrain conditions have been implemented. The effect due to whole set of damage (highlighted by the circles in Fig. 8) has been simultaneously taken into account in the modal strain energy evaluation. It is worth to note that the presented damage configuration in some way covers the critical zones of the panel, that is to say, the edges and the inner area. Due to the optimized path of the fiber optic, running also along the perimeter 4 impacts fall very close to sensor. The other 2 inner impacts, very close each other, give the opportunity of qualitatively appreciating the spatial resolution capability of the sensor.

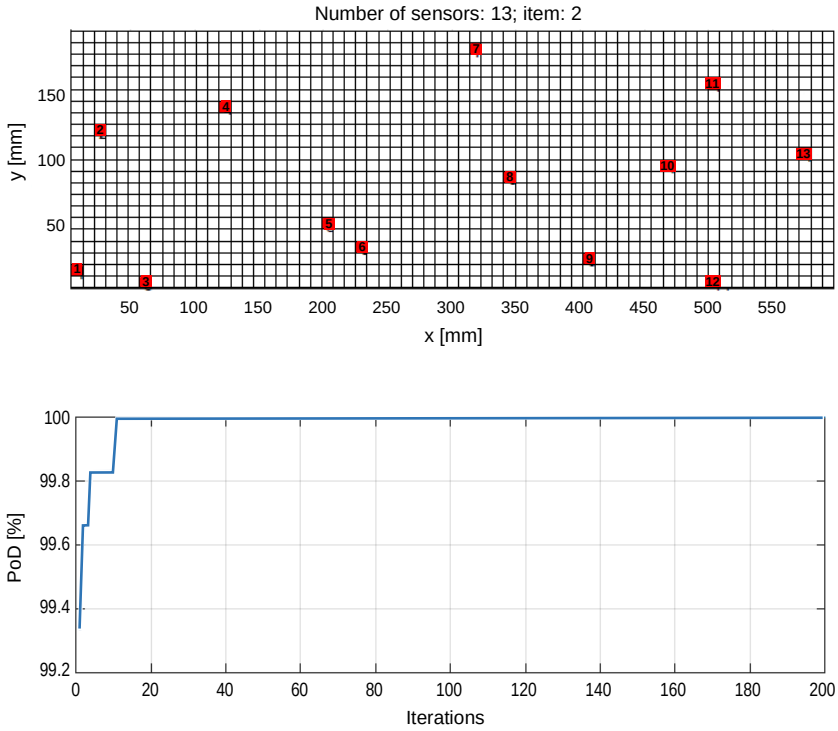

Fig. 5. Optimized configurations and PoD evolutions for 13 sensors

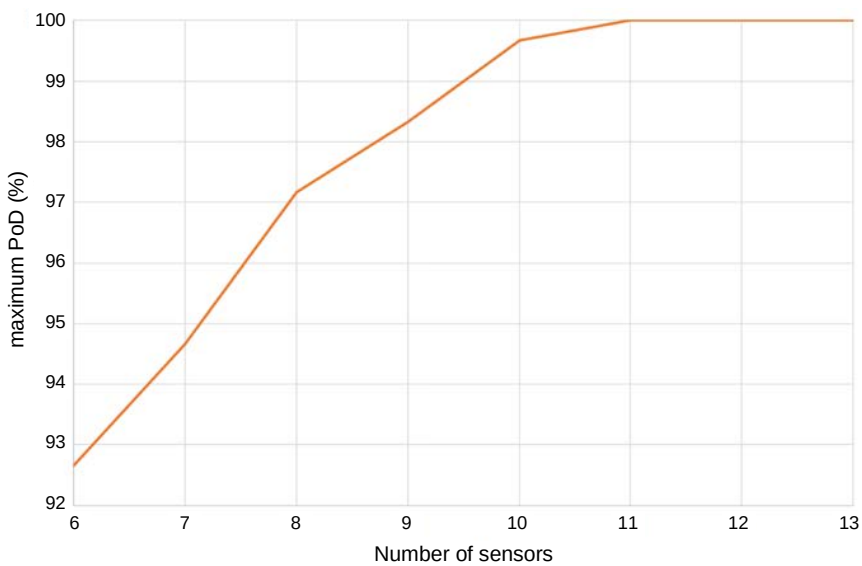

Fig. 6. Maximum PoD vs. number of sensors

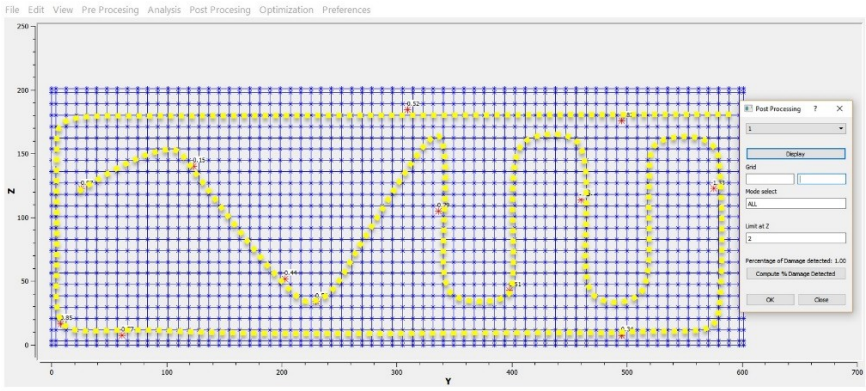

Fig. 7. Damage Index values at baseline (no strain) by optimal fiber optic strain sensor layout

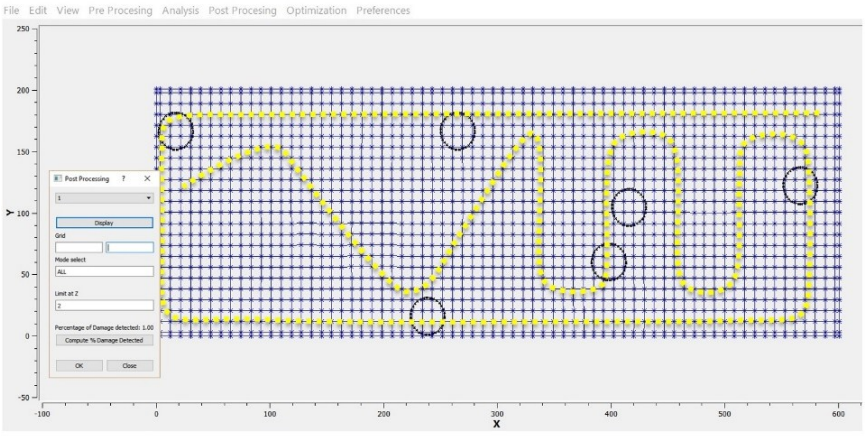

Fig. 8. Fiber optic layout with a damage impact position. The circle indicating the 20 mm diameter of a BVID impact area due to a low energy (50 J) impact

For each impact, the closer sensors to the impact locations provide a DI alert ($z > 2$), as expected by the strain energy approach (see Fig. 9).

Since the panel taken into account is representative of an aeronautic skin element, only the first two bending and torsional modes have been considered, as the most relevant ones for a typical aeronautical panel.

In Fig. 9, the color plot of the strain energy of the damaged plate is reported with reference to its baseline healthy state. The color plot indicates the modal strain energy values along the fiber optic, corresponding to a damage index value ($z > 2$ is assumed as threshold value). The generation of the graph has been performed by interpolating the experimental sensor readings. To this scope, a dedicated function has been implemented to provide the damage index value. Each time the threshold is overshot, (blue to green range, corresponding to the calibration of the healthy plate) a structural damage is associated to a color gradient (green to red range).

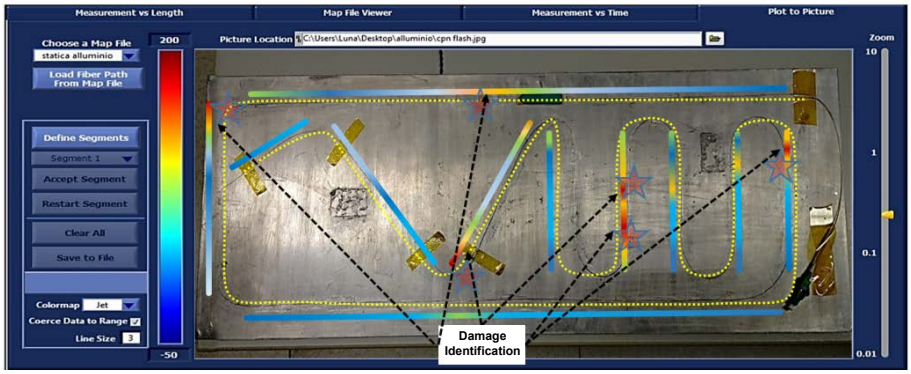

Fig. 9. Detection of damage by optimal sensor network layout

It is worth to note that during the impacts, the last segment of the fiber optic has been broken, but the fiber repair has been possible by fusion splicing (see Fig. 9).

5. Anisotropic test case: composite plate

A composite stiffened plate has been considered. The material is an orthotropic carbon fiber with a Young's modulus in fiber direction equal to $E_1 = 137500$ MPa and a Young's modulus in matrix direction equal to $E_2 = 8200$ MPa. The skin has a rectangular shape, 450 mm long, 500 mm wide and 5 mm thick. The sequence of lamination is symmetrical and balanced with a total number of 24 ply. The stringer cap is 450 mm long, 67.3 mm wide and 2.5 mm thick. The sequence of lamination, symmetric and balanced, is as follows: $[0, 90, 0, 0, -45, 45]_s$ with a total number of 12 ply. The experimental damage condition is a skin-stringer delamination.

When considering a composite stiffened plate, the skin-stringer bonding lines integrity is of great interest. The skin-stringer debonding can occur in different ways, depending, to cite some examples, on the type of load, its magnitude and its time duration. For this reason, the damaged areas random generated have been supposed to be located close or inside the interface between the panel and one stiffener (the second starting from the top row of Fig. 10). The database used for the simulation was built by simply changing the extension of the debonding area. The scheme reported in Fig. 10 illustrates the types of damage taken into account (on the boundary or inside). The finite elements included in the damage area domains are suitably modified, according to the approach described in section 2.

Ten different initial populations have been generated. The PoD has been computed considering the first 4 modes. In Fig. 11, the evolution of the PoD is shown per each of these initial populations. The optimization parameters, in this case, are represented by the in plane coordinates of the edges of two straight lines, constituting the go and back path of the fiber. As mentioned in section 1, a check has been

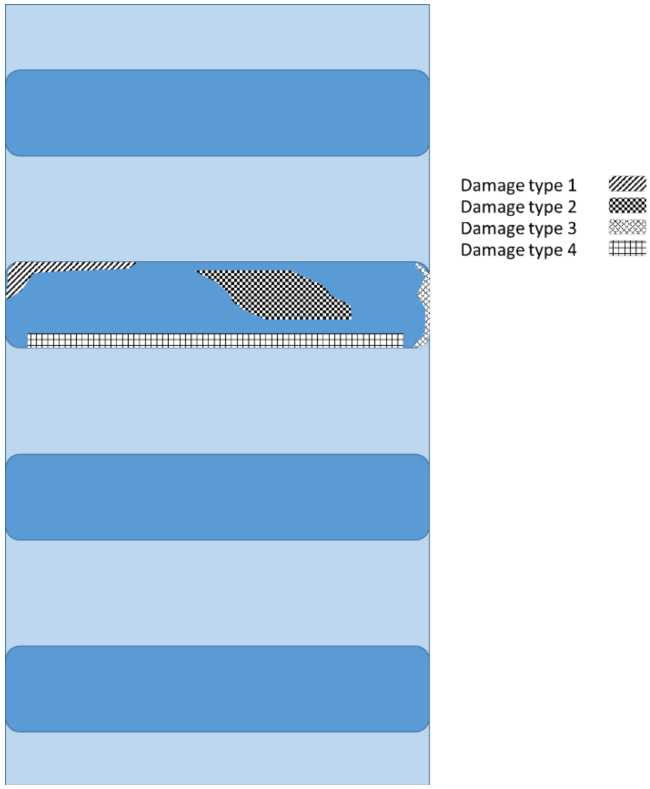

Fig. 10. Types of damage considered at the second top stiffener interface

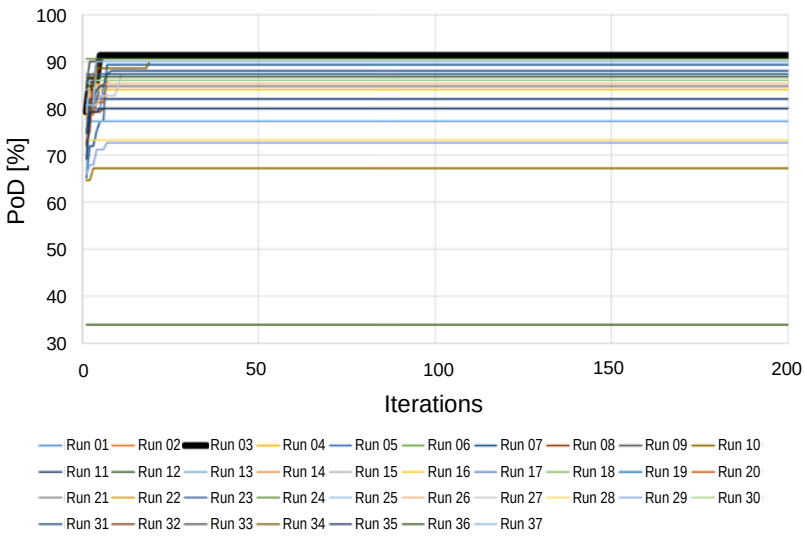

Fig. 11. PoD evolution vs. run (initial population)

foreseen to discharge any layout intersecting the bonded domain. The most runs has been converged to PoD values between 80 and 90%.

The optimal layout provided by the genetic algorithm, corresponds to the fiber optic along the stringer cap bonding line. The strain sensors are expected to exhibit higher values of DI in case of a skin-stringer debonding. Despite the high density of the sensing points provided by the distributed fiber optic (the fiber used has a spatial resolution of 5 mm), for the sake of clearness, only few labels of z were reported in Fig. 12.

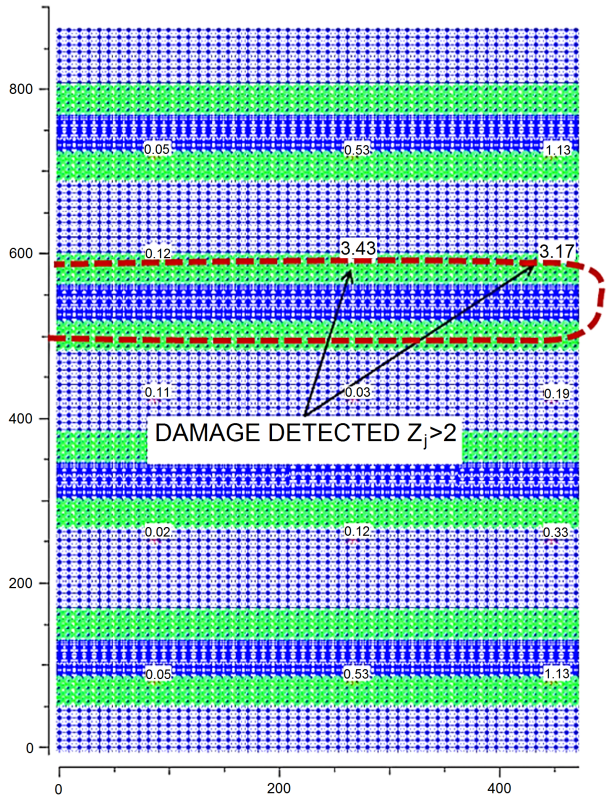

Fig. 12. Damage Index values provided by optimal fiber optic strain path (dotted line)

A single impact has been provided on the skin; the image of the stringer debonding section is reported in Fig. 13.

Due to the stiffener of the plate (second resonance > 300 Hz), the modal approach has been ineffective, being the instrumentation max sampling rate capability 250 Hz. This is the reason why, in this specific application, a static bending solicitation, simulating a first bending mode, has been provided. The damage index in this case has been computed on the basis of the strain map of this single shape. Fig. 14 is an image of the differential strain level, with respect to the unloaded condition, detected by the optical interrogator.

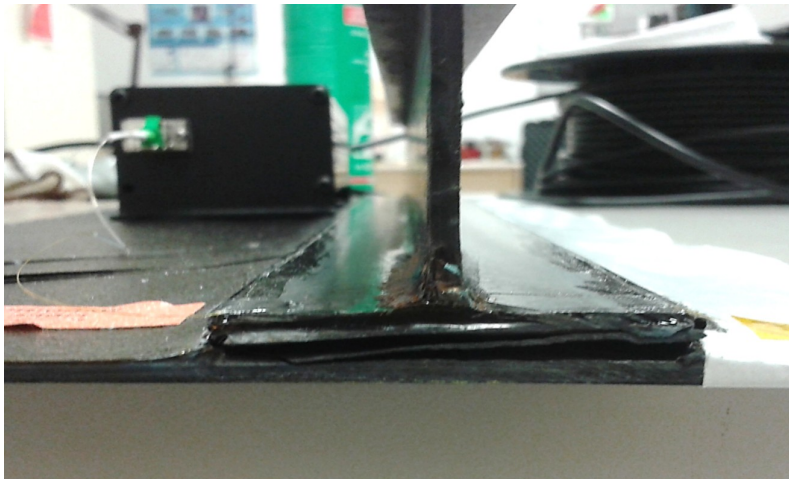

Fig. 13. Skin-stringer debonded detail

The sensor is 1 m long, enough to monitor the stringer perimeter, that is to say, the both caps. The almost flat curve of Fig. 14, corresponds to a undamaged semi-cap, while the irregular strain distribution highlights a dispersion trend of the measure along the other semi-cap.

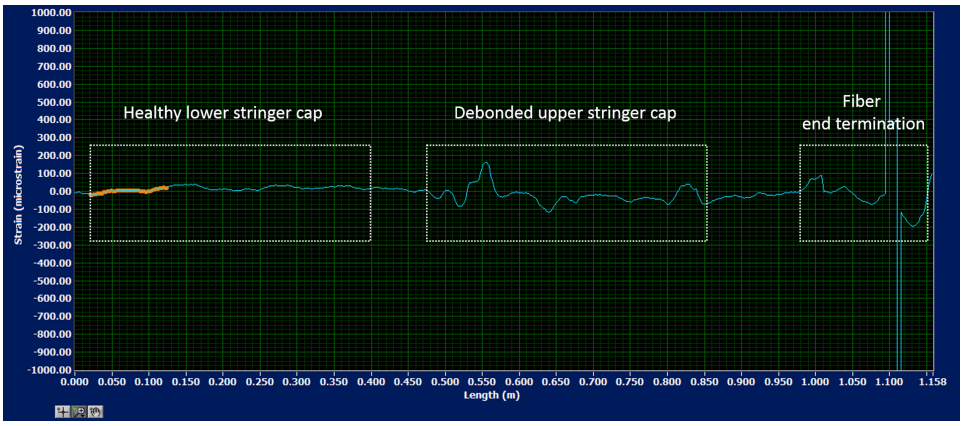

Fig. 14. Bonding line strain values along the fiber optic

The structural health of the plate has been verified and confirmed by visual inspection (Fig. 13). The numerical simulation (Fig. 12) is in agreement with the experimental results. The z values provided by the methodology have been higher along the damaged semi-cap.

6. Conclusions

An optimization process has been defined and implemented to determine the path according which the fiber optic should be laid over the reference elements. In this preliminary phase, a classic strain energy approach has been adopted as well established damage detection criteria providing a damage index alert for a random dataset of damage. Then, a genetic-based algorithm has provided the optimal sensor network layout by maximizing the PoD function.

The methodology has been validated, by means of two aeronautical panels (flat metal and composite stiffened panels), both carrying typical damage scenarios: impact and debonding.

In the first test case, after having instrumented the plate according to the optimization process, different impacts have been exerted. In this application, the fiber optic has successfully detected the location of the damage network.

In the second test case, a skin-stringer debonding has been occurred after impact. The sensor optimization has provided with a straight path constraint. Again, the fiber bonded above the stringer cap, has proved to be sensitive enough to detect damage extension.

The preliminarily results demonstrated the goodness of the selected methodology, but an assessment of the process is necessary to demonstrate the reliability of the general approach.

Manuscript received by Editorial Board, May 18, 2018;
final version, January 14, 2019.

References

[1] C. Boller, F.K. Chang, and Y. Fujino. *Encyclopedia of Structural Health Monitoring*. John Wiley & Sons Ltd., Chichester, UK, 2009.

[2] M.I. Friswell. Damage identification using inverse methods. *Philosophical Transactions of the Royal Society A: Mathematical, Physical and Engineering Sciences*, 365(1851):393–410, 2007. doi: 10.1098/rsta.2006.1930.

[3] S. Zhou, Y. Bao, and H. Li. Optimal sensor placement based on substructure sensitivity. In *Proceedings of SPIE, Sensors and Smart Structures Technologies for Civil, Mechanical, and Aerospace Systems*, volume 8345, 2012. doi: 10.1117/12.915074.

[4] D.C. Kammer and M.L. Tinker. Optimal placement of triaxial accelerometers for modal vibration tests. *Mechanical Systems and Signal Processing,* 18(1):29–41, 2004. doi: 10.1016/S0888-3270(03)00017-7.

[5] M. Najeeb and V. Gupta. Energy efficient sensor placement for monitoring structural health. *International Electronic Conference on Sensors and Applications*, 1–16 June 2014. doi: 10.3390/ecsa-1-d008.

[6] W. Liu, W.C. Gao, Y. Sun, and M.J. Xu. Optimal sensor placement for spatial lattice structure based on genetic algorithms. *Journal of Sound and Vibration* 317(1–2):175–189, 2008. doi: 10.1016/j.jsv.2008.03.026.

[7] H. Gao and J.L. Rose. Sensor placement optimization in structural health monitoring using genetic and evolutionary algorithms. *Proceedings of SPIE, Sensors and Smart Structures Technologies for Civil, Mechanical, and Aerospace Systems*, volume 6174, 2006. doi: 10.1117/12.657889.

[8] X. Bao and L. Chen. Recent progress in Brillouin scattering based fiber sensors. *Sensors*, 11(4):4152–4187, 2011. doi: 10.3390/s110404152.

[9] L. Maurin, P. Ferdinand, F. Nony, and S. Villalonga. OFDR distributed strain measurements for SHM of hydrostatic stressed structures: an application to high pressure hydrogen storage type IV composite vessels – H2E Project. *7th European Workshop on Structural Health Monitoring*, pages 930–937, Nantes, France, 8–11 July, 2014.

[10] O. Shapira, U. Ben-Simon, A. Bergman, S. Shoham, B. Glam, I. Kressel, T. Yehoshula, and M. Tur. Structural health monitoring of a UAV fleet using fiber optic distributed strain sensing. *International Workshop on Structural Health Monitoring*, Stanford, CA, USA, 1–3 September, 2015. doi: 10.12783/SHM2015/371.

[11] J. Li, R.K. Kapania, and W. B. Spillman. Placement optimization of distributed-sensing fiber optic sensors using genetic algorithms, *AIAA Journal*, 46(4):824–836, 2008. doi: 10.2514/1.25090.

[12] H. Li, H. Yang, and S.-L.J, Hu. Modal strain energy decomposition method for damage localization in 3D frame structures. *Journal of Engineering Mechanics*, 132(9):41–951, 2006. doi: 10.1061/(ASCE)0733-9399(2006)132:9(941).

[13] H.-W. Hu and C.-B. Wu. Non-destructive damage detection of two dimensional plate structures using modal strain energy method. *Journal of Mechanics*, 24(4):319–332, 2008. doi: 10.1017/S1727719100002458.

[14] Z.Y. Shi, S.S. Law, and L.M. Zhang. Improved damage quantification from elemental modal strain energy change. *Journal of Engineering Mechanics*, 128(5):521–529, 2002. doi: 10.1061/(ASCE)0733-9399(2002)128:5(521).

[15] M. Ciminello, A. Concilio, B. Galasso, and F.M. Pisano. Skin-stringer debonding detection using distributed dispersion index features. *Structural Health Monitoring*, 17(5):1245–1254, 2018. doi: 10.1177/1475921718758980.

[16] P.O. Mensah-Bonsu. *Computer-aided Engineering Tools for Structural Health Monitoring under Operational Conditions*. Master's Thesis, University of Connecticut, USA, 2012. doi: https://digitalcommons.uconn.edu/gs_theses/278.

[17] R. Mason, L.A. Ginter, M. Singleton, V.F. Hock, R.G Lampo, and S.C. Sweeney. A novel integrated monitoring system for structural health management of military infrastructure, *Proceedings of Department of Defense Corrosion Conference*, 2009.

[18] S. Beskhyroun. Graphical interface toolbox for modal analysis. *Proceedings of the Ninth Pacific Conference on Earthquake Engineering: Building an Earthquake-Resilient Society*, Auckland New Zealand, 14–16 April 2011.